

## REMOTE EFFECTS SPATIAL PROCESS MODELS FOR MODELING TELECONNECTIONS

BY JOSHUA HEWITT<sup>\*</sup> , JENNIFER A. HOETING<sup>\*</sup> , JAMES M. DONE<sup>†</sup>  
AND ERIN TOWLER<sup>†</sup>

*Colorado State University<sup>\*</sup> and National Center for Atmospheric Research<sup>†</sup>*

**Abstract:** Precipitation is one example of an important, local climatic process that is influenced by remote covariates, like sea surface temperature, as well as local covariates, like surface air temperature. Remote influences on climate are called teleconnection effects and often arise from complex interactions between the atmosphere and ocean, of which the El Niño–Southern Oscillation teleconnection is a relevant, well-known example. Teleconnection effects are known to improve predictions of precipitation patterns, but many statistical methods that incorporate teleconnection effects do not directly account for spatial dependence or local covariates in estimation. We introduce a model that provides statistically valid inference and improved prediction as compared to methods commonly used to analyze spatially-referenced data that is influenced by local and remote covariates. Our model draws on ideas from spatially varying coefficient models, spatial basis functions, and predictive processes to overcome modeling challenges for teleconnections. As a general result, we extend the standard geostatistical modeling framework to account for effects of covariates observed on a spatially remote domain. We adopt a hierarchical Bayesian framework to conduct inference and make predictions; the method is demonstrated by predicting precipitation in Colorado and accounts for teleconnection effects with Pacific Ocean sea surface temperatures. We show how the proposed model improves upon standard methods for estimating teleconnection effects and discuss its utility for climate downscaling applications.

**1. Introduction.** Precipitation is critical for many sectors of society and ecological systems. As such, there has been great interest and research towards understanding precipitation variability and change at long time scales. Direct precipitation prediction by global climate models (GCMs) is challenging because of complex and interacting multi-scale physical precipitation processes. This has resulted in large uncertainty in future changes in precipitation patterns (e.g., [Deser et al., 2012](#)). Even the sign of future precipitation change is uncertain ([Tignor et al., 2013](#)). This uncertainty arises from different GCMs giving different precipitation responses to a given cli-

---

*Keywords and phrases:* spatial, climate, teleconnection, hierarchical, Bayesian, EOF

mate state, the same GCM giving different precipitation responses to different initial conditions, and uncertainty in the given climate state (Hawkins and Sutton, 2010). While GCMs perform poorly in predicting precipitation directly, they can skillfully reproduce surface temperatures and large-scale patterns (Flato et al., 2013) that, in turn, affect precipitation. Statistical downscaling methods can use these large-scale patterns to improve predictions in some regions (Goddard et al., 2001).

Large-scale patterns of sea surface temperature (SST) or geopotential height, for example, can influence temperature and precipitation in regions remote to the pattern's source. Phenomena like this are called teleconnections and induce statistical dependence between remote regions. For example, several seminal studies connect U.S. precipitation with SST anomalies due to the El Niño–Southern Oscillation teleconnection (ENSO) (Ting and Wang, 1997; Montroy, 1997; Montroy, Richman and Lamb, 1998). Teleconnections have been exploited to improve predictions of precipitation at varied spatial and temporal scales. Teleconnections have been critical in seasonal climate forecasting (Goddard et al., 2001) as well as in statistical downscaling of current and future climates simulated by GCMs. This paper builds on our understanding of statistical downscaling of precipitation at long time scales by proposing a geostatistical model that accounts for spatial dependence and influence of both remote and local effects.

Statistical downscaling methods relate local or regional variables to large-scale variables. One class of statistical downscaling methods is “perfect prognosis downscaling” (Maraun et al., 2010), whereby a statistical relationship is developed between observed large-scale predictors and local-scale weather phenomena (e.g., Wilby et al., 1998; Bruyere, Holland and Towler, 2012; Towler, PaiMazumder and Holland, 2016). Once these relationships are developed on observed datasets, they can be applied to large-scale GCM data to obtain finer scale information through prediction. Clearly, this approach is highly dependent on the quality and predictive nature of the selected predictors (Fowler, Blenkinsop and Tebaldi, 2007).

Since regional precipitation largely arises from a combination of local and remote interactions that occur between atmospheric (e.g., pressure levels, water vapor content, surface air temperature), oceanic (e.g., sea surface temperature), and orographic (e.g., elevation, slope, aspect) factors, a hybrid approach is important for its prediction. However, many statistical downscaling models that account for remote, teleconnection effects do not also comprehensively account for local effects or spatial dependence. Common models are based on pointwise linear regressions or multivariate methods, like canonical correlation analysis, that use empirical covariances (van den

Dool, 2007, Chapters 8, 9). Similarly, standard statistical models that comprehensively account for spatial dependence are only designed to account for local effects and cannot readily incorporate remote, teleconnection effects (cf. Banerjee, Carlin and Gelfand, 2015, Chapters 6, 9, 11). While Choi et al. (2015) propose a spatially-motivated model that is similar to canonical correlation analysis, but adapted to incorporate spatial dependence, their method does not consider local covariates. Choi et al. (2015) study teleconnection by analyzing cross-covariance matrices smoothed by spatial basis functions. This paper, by comparison, proposes to improve statistical downscaling by extending geostatistical models to incorporate teleconnection principles.

We propose a geostatistical model for teleconnection, which represents a class of spatial analysis problems that standard geostatistical models do not consider. Figure 1 schematically illustrates the general teleconnection problem in which local  $X(s, t)$  and remote  $Z(r, t)$  covariates impact a local spatio-temporal response  $Y(s, t)$ . The remote effects spatial process (RESP) model we propose extends standard spatial models to account for the influence of covariates observed on a geographically remote domain  $Z(r, t)$ .

As we will show below, the RESP model provides statistically valid inference as well as more accurate predictions as compared with standard methods. The RESP model is hierarchical and directly accounts for spatial dependence in estimating teleconnection effects, which comprehensively mitigates several significance testing issues raised in prior work. The seminal studies of teleconnection mentioned above use varied and sometimes ad-hoc resampling and Monte Carlo techniques to indirectly account for spatial dependence and sampling-related issues when building statistical evidence for the existence of teleconnection phenomena between large-scale patterns and a local response. Many of these methods are limited, however, and cannot provide correction to local estimates of teleconnection. When significance of local effects is reported, it is often reported pointwise without corrections for spatial dependence. By comparison, the RESP model provides a model-based framework to estimate teleconnection effects while simultaneously accounting for spatial dependence.

As a tool for statistical downscaling, our RESP model can produce accurate predictions. We demonstrate the model by predicting Colorado winter precipitation for target years with given values of winter covariates at the same timepoints. This approach is a type of perfect prognosis downscaling, and could be applied to make predictions by using covariates that have been forecasted or simulated by GCMs, for example. Atmospheric processes have relatively short memory, thus it is reasonable to assume that winter precipitation is conditionally independent across years. Therefore, we develop our

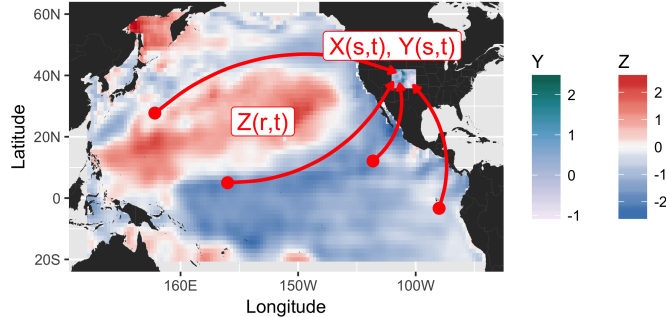


FIG 1. Schematic illustration of a teleconnection problem. Colorado precipitation  $Y(s, t)$  is influenced by both local covariates  $\mathbf{X}(s, t)$  and remote covariates  $Z(r, t)$ . The remote covariates shown here are standardized anomalies of average monthly Pacific Ocean sea surface temperatures during Winter, 1988. The data come from the ERA-Interim reanalysis dataset (Dee et al., 2011).

RESP model assuming there is no meaningful temporal dependence.

We introduce our teleconnection model in the more general context of a spatial regression problem involving local and spatially remote covariates (Section 2), then demonstrate in a cross-validation study that it predicts Colorado winter precipitation better than standard downscaling methods (Section 3). We conclude with directions for future work and further application (Section 4).

**2. A geostatistical model for spatially remote covariates.** We introduce the RESP model in Sections 2.1 to 2.3. In particular, we discuss constraints (Section 2.2) that need to be applied to the model's initial formulation (Section 2.1) as well as connections between the RESP model and existing approaches for measuring teleconnection (Section 2.3). We discuss inference in Sections 2.4 to 2.7, including the model likelihood (Section 2.4), Bayesian approach for estimation (Sections 2.5 and 2.6), and assessment (Section 2.7).

**2.1. Model formulation.** We introduce the remote effects spatial process (RESP) model to extend the standard geostatistical setting in which a local response variable  $Y(s, t) \in \mathbb{R}$  and known covariate vector  $\mathbf{x}(s, t) \in \mathbb{R}^p$  are observable at discrete timepoints  $t \in \mathcal{T} = \{t_1, \dots, t_{n_t}\}$  and at locations  $s$  in a continuous domain  $\mathcal{D}_Y$ . The RESP model includes the effects of known remote covariates  $z(r, t) \in \mathbb{R}$ , which are observable at locations  $r$  in a spatially disjoint continuous domain—i.e., in a continuous  $\mathcal{D}_Z$  s.t.

$\mathcal{D}_Y \cap \mathcal{D}_Z = \emptyset$ . The RESP model is given by

$$(1) \quad Y(\mathbf{s}, t) = \mathbf{x}^T(\mathbf{s}, t)\boldsymbol{\beta} + w(\mathbf{s}, t) + \varepsilon(\mathbf{s}, t) + \gamma(\mathbf{s}, t)$$

where the regression coefficients  $\boldsymbol{\beta} \in \mathbb{R}^p$ , spatially correlated noise  $w(\mathbf{s}, t)$ , and independent noise  $\varepsilon(\mathbf{s}, t)$  are standard components for spatial regression models (cf. [Banerjee, Carlin and Gelfand, 2015](#), Chapters 6, 9, 11). In the RESP model the teleconnection effect given by  $\gamma(\mathbf{s}, t)$  is defined by

$$(2) \quad \gamma(\mathbf{s}, t) = \int_{\mathcal{D}_Z} z(\mathbf{r}, t) \alpha(\mathbf{s}, \mathbf{r}) d\mathbf{r}$$

which describes the net effect of the remote covariates  $z(\mathbf{r}, t)$  on the continuous spatial process  $Y(\mathbf{s}, t)$  at discrete time  $t$ . The integral (2) reduces to a sum in finite samples, in which the remote covariates  $z(\mathbf{r}, t)$  are observed at  $n_r < \infty$  locations. The remote (or teleconnection) coefficients  $\alpha(\mathbf{s}, \mathbf{r})$  are spatially correlated and doubly-indexed by  $(\mathbf{s}, \mathbf{r}) \in \mathcal{D}_Y \times \mathcal{D}_Z$ . The spatial correlation and double-indexing of  $\alpha(\mathbf{s}, \mathbf{r})$  represents teleconnection effects that vary regionally in the sense that the response  $Y(\mathbf{s}, t)$  at one location  $\mathbf{s} \in \mathcal{D}_Y$  can respond to the remote covariates  $z(\mathbf{r}, t)$  more strongly than the response  $Y(\mathbf{s}', t)$  at another location  $\mathbf{s}' \in \mathcal{D}_Y$ . Similarly, the response  $Y(\mathbf{s}, t)$  at one location  $\mathbf{s} \in \mathcal{D}_Y$  can respond differently to remote covariates  $z(\mathbf{r}, t)$  and  $z(\mathbf{r}', t)$  at distinct remote locations  $\mathbf{r}, \mathbf{r}' \in \mathcal{D}_Z$ . Thus, the remote coefficients  $\alpha(\mathbf{s}, \mathbf{r})$  vary spatially and use the remote covariates  $z(\mathbf{r}, t)$  to provide local adjustment to the mean response. The teleconnection term  $\gamma(\mathbf{s}, t)$  is well defined since we assume the remote covariates  $z(\mathbf{r}, t)$  are known and square-integrable over  $\mathcal{D}_Z$  at each timepoint  $t$  ([Adler and Taylor, 2007](#), Section 5.2).

The RESP model provides a simple geostatistical approach to modeling teleconnections by extending spatial regression models to incorporate data from spatially remote regions. The teleconnection term  $\gamma(\mathbf{s}, t)$  distinguishes the RESP model (1) from standard geostatistical models, in which—for example—the responses  $Y(\mathbf{s}, t)$  and  $Y(\mathbf{s}', t)$  at distinct spatial locations  $\mathbf{s}, \mathbf{s}' \in \mathcal{D}_Y$  are only influenced by distinct covariates  $x(\mathbf{s}, t)$  and  $x(\mathbf{s}', t)$ . To model the influence of teleconnection phenomena the RESP model lets the remote covariates  $z(\mathbf{r}, t)$  simultaneously influence the responses  $Y(\mathbf{s}, t)$  and  $Y(\mathbf{s}', t)$ .

Geostatistical modeling conventions use mean zero Gaussian processes to specify the randomness of the unknown, spatially correlated components  $w(\mathbf{s}, t)$  and  $\alpha(\mathbf{s}, \mathbf{r})$ , and an independent processes to specify the noise  $\varepsilon(\mathbf{s}, t)$ —the nugget. We complete the Gaussian process specifications by defining the covariance functions for the spatially correlated components.

Let  $C_w$  and  $C_\alpha$  respectively be the covariance functions for  $w(\mathbf{s}, t) + \varepsilon(\mathbf{s}, t)$  and  $\alpha(\mathbf{s}, \mathbf{r})$ , where

$$(3) \quad C_w \{(\mathbf{s}, t), (\mathbf{s}', t')\} = (\kappa(\mathbf{s}, \mathbf{s}'; \boldsymbol{\theta}_w) + \sigma_\varepsilon^2 \delta_{\mathbf{s}, \mathbf{s}'}) \delta_{t, t'},$$

$$(4) \quad C_\alpha \{(\mathbf{s}, \mathbf{r}), (\mathbf{s}', \mathbf{r}')\} = (\kappa(\mathbf{s}, \mathbf{s}'; \boldsymbol{\theta}_w) + \sigma_\varepsilon^2 \delta_{\mathbf{s}, \mathbf{s}'}) \kappa(\mathbf{r}, \mathbf{r}'; \boldsymbol{\theta}_\alpha).$$

Here we assume  $\kappa$  represents the stationary Matérn covariance

$$(5) \quad \kappa(\mathbf{u}, \mathbf{v}; \boldsymbol{\theta}) = \frac{\sigma^2}{2^{\nu-1} \Gamma(\nu)} (d(\mathbf{u}, \mathbf{v}) / \rho)^\nu K_\nu(d(\mathbf{u}, \mathbf{v}) / \rho)$$

for spatial locations  $\mathbf{u}$  and  $\mathbf{v}$ , and parameter vector  $\boldsymbol{\theta} = (\sigma^2, \rho, \nu)^T$ . The function  $d(\mathbf{u}, \mathbf{v})$  is an appropriate distance function (e.g., great-circle distances for locations on a sphere),  $\sigma^2 > 0$  is a scaling parameter,  $\nu > 0$  is a smoothness parameter,  $\rho > 0$  is a range parameter, and  $K_\nu$  is the modified Bessel function of the second kind with order  $\nu$ . In covariance function definitions (3) and (4),  $\delta$  represents the Kronecker delta function and  $\sigma_\varepsilon^2$  represents the variance of the nugget process which we specify to be a collection of independent and identically distributed mean zero Gaussian random variables—i.e.,  $\varepsilon(\mathbf{s}, t) \stackrel{iid}{\sim} \mathcal{N}(0, \sigma_\varepsilon^2) \quad \forall (\mathbf{s}, t) \in \mathcal{D}_Y \times \mathcal{T}$ .

While the definitions (3) and (4) for the local and remote covariances  $C_w$  and  $C_\alpha$  can be generalized, the definitions restrict our use of the RESP model to working in the perfect prognosis downscaling setting described at the end of Section 1. The responses  $Y(\mathbf{s}, t)$  and  $Y(\mathbf{s}, t')$  for  $t \neq t'$  are independent given covariates and sufficiently separated timepoints, like successive winters (e.g., winter 1991, winter 1992, etc.). The remote covariance  $C_\alpha$  also induces a separable structure for the remote coefficients  $\alpha(\mathbf{s}, \mathbf{r})$ , which constrains the spatial variability of teleconnection effect fields and simultaneously constrains the teleconnection effects  $\{\alpha(\mathbf{s}, \mathbf{r}) : \mathbf{r} \in \mathcal{D}_Z\}$  and  $\{\alpha(\mathbf{s}', \mathbf{r}) : \mathbf{r} \in \mathcal{D}_Z\}$  to be similar for nearby locations  $\mathbf{s}$ ,  $\mathbf{s}' \in \mathcal{D}_Y$ . Simpler covariance structures for the teleconnection effects  $\alpha(\mathbf{s}, \mathbf{r})$  may not capture these physical properties of teleconnection as directly. Similarly, although climate data are often available as gridded data products, we choose to work with geostatistical covariance models instead of autoregressive spatial models that incorporate the discrete nature of spatial gridded data so that we may avoid inducing potentially counterintuitive covariance structures (see, e.g., [Wall, 2004](#); [Assunção and Krainski, 2009](#)).

**2.2. Reduced rank approximation.** To apply the RESP model (1), additional constraints need to be imposed due to the potential multicollinearity in the covariates. Remote covariates  $z(\mathbf{r}, t)$  in teleconnection applications

will often consist of data that measure ocean properties at high spatial resolution, like sea surface temperature or sea level pressure. This raises concerns for estimating the remote coefficients  $\alpha(\mathbf{s}, \mathbf{r})$  in (2) as the main trends in the remote covariates  $z(\mathbf{r}, t)$  are highly collinear over  $\mathcal{D}_Z$ . Physically, however, this suggests the remote coefficients should be highly correlated as well. We use predictive processes to mitigate multicollinearity in the remote covariates, which is an alternative motivation for predictive processes. [Banerjee et al. \(2008\)](#) originally introduce predictive processes so that parameters of geostatistical models can be estimated for large spatial datasets, rather than as an approach for mitigating spatial multicollinearity.

We assume the remote coefficients  $\alpha(\mathbf{s}, \mathbf{r})$  can be well represented by weighted averages of remote coefficients  $\alpha(\mathbf{s}, \mathbf{r}^*)$  at knot locations

$\mathbf{r}_1^*, \dots, \mathbf{r}_k^* \in \mathcal{D}_Z$ , so we make the simplifying approximation that for some weight function  $h(\mathbf{r}, \mathbf{r}')$  and associated vector  $\mathbf{h}^*(\mathbf{r}) = [h(\mathbf{r}, \mathbf{r}_j^*)]_{j=1}^k \in \mathbb{R}^k$  we can write

$$(6) \quad \alpha(\mathbf{s}, \mathbf{r}) = \sum_{j=1}^k h(\mathbf{r}, \mathbf{r}_j^*) \alpha(\mathbf{s}, \mathbf{r}_j^*) = \mathbf{h}^*(\mathbf{r})^T \boldsymbol{\alpha}^*(\mathbf{s}),$$

where  $\boldsymbol{\alpha}^*(\mathbf{s}) = [\alpha(\mathbf{s}, \mathbf{r}_j^*)]_{j=1}^k \in \mathbb{R}^k$ . The predictive process approach uses kriging to motivate a choice for the weight vector  $\mathbf{h}^*(\mathbf{r})$ , which induces a weight function  $h$ . Using Gaussian processes in Section 2.1 to model the remote coefficients implies that  $\alpha(\mathbf{s}, \mathbf{r})$  and  $\boldsymbol{\alpha}^*(\mathbf{s})$  are jointly normally distributed, yielding the conditional expectation for  $\alpha(\mathbf{s}, \mathbf{r})$

$$(7) \quad E[\alpha(\mathbf{s}, \mathbf{r}) | \boldsymbol{\alpha}^*(\mathbf{s})] = \mathbf{c}^*(\mathbf{r})^T R^{*-1} \boldsymbol{\alpha}^*(\mathbf{s})$$

in which  $\mathbf{c}^*(\mathbf{r}) = [C_\alpha\{(\mathbf{s}, \mathbf{r}), (\mathbf{s}, \mathbf{r}_j^*)\}]_{j=1}^k \in \mathbb{R}^k$  and  $R^* \in \mathbb{R}^{k \times k}$  with entries  $R_{ij}^* = C_\alpha\{(\mathbf{s}, \mathbf{r}_i^*), (\mathbf{s}, \mathbf{r}_j^*)\}$ . Note that the assumption in (4) that  $C_\alpha$  is stationary means that  $\mathbf{c}^*(\mathbf{r})$  and  $R^*$  do not depend on  $\mathbf{s}$ , despite the term appearing in their definitions.

The predictive process approach uses the conditional expectation (7) to define the weight vector  $\mathbf{h}^*(\mathbf{r}) = \mathbf{c}^*(\mathbf{r})^T R^{*-1}$  in the approximation (6). [Banerjee et al. \(2008\)](#) show that these types of approximations are reduced rank projections that can capture key spatial structures in data and are optimal with respect to the Kullback-Leibler divergence.

Beyond mitigating the statistical issue of multicollinearity, this approach also has a physical interpretation for teleconnection. Using the reduced rank

approximation (6) to manipulate the integral in (1) shows that the reduced rank approximation can be interpreted as inducing transformed covariates  $z^*(\mathbf{r}^*, t)$  via

$$(8) \quad \begin{aligned} \int_{\mathcal{D}_Z} z(\mathbf{r}, t) \alpha(\mathbf{s}, \mathbf{r}) d\mathbf{r} &= \int_{\mathcal{D}_Z} z(\mathbf{r}, t) \sum_{j=1}^k h(\mathbf{r}, \mathbf{r}_j^*) \alpha(\mathbf{s}, \mathbf{r}_j^*) d\mathbf{r} \\ &= \sum_{j=1}^k \alpha(\mathbf{s}, \mathbf{r}_j^*) z^*(\mathbf{r}_j^*, t) \end{aligned}$$

where  $z^*(\mathbf{r}_j^*, t) = \int_{\mathcal{D}_Z} z(\mathbf{r}, t) h(\mathbf{r}, \mathbf{r}_j^*) d\mathbf{r}$ . Thus, using the predictive process approach to address multicollinearity in the remote covariates is analogous to reducing the remote covariates  $z(\mathbf{r}, t)$ ,  $\mathbf{r} \in \mathcal{D}_Z$  at each timepoint to  $k$  spatially-averaged indices  $z^*(\mathbf{r}^*, t)$  centered at  $\mathbf{r}^*$  for  $\mathbf{r}^* \in \{\mathbf{r}_1^*, \dots, \mathbf{r}_k^*\}$ . This manipulation is fairly generic and should be applicable to all predictive process models. For teleconnection, this manipulation connects the RESP model to one set of standard teleconnection methodologies (cf. [Ashok et al., 2007](#); [Towler, PaiMazumder and Holland, 2016](#)), in which teleconnection effects are measured with respect to ocean indices based on spatial averages of remote covariates rather than to individual remote covariates as the RESP model does in its definition (1).

**2.3. Spatial basis function transformation of remote coefficients.** The RESP model (1) is also related to another set of standard teleconnection methodologies (cf. [Ting and Wang, 1997](#); [Montroy, 1997](#)), in which teleconnection effects are measured with respect to complex ocean indices such as empirical orthogonal functions. Spatial basis functions provide a means to reparameterize the RESP model and show it can identify and leverage known teleconnections with complex patterns. We will use the following reparameterization of the teleconnection effects  $\alpha(\mathbf{s}, \mathbf{r})$  to discuss teleconnection between Pacific Ocean sea surface temperature and Colorado precipitation in Section 3.

Complex teleconnection patterns are often based on spatial basis function expansions of the remote covariates  $z(\mathbf{r}, t)$ . If there exist weights  $\{a_l(t) : l = 1, \dots, K; t \in \mathcal{T}\}$  such that the remote covariates  $z(\mathbf{r}, t)$  can be written as a linear combination of time-invariant basis functions  $\{\psi_l(\mathbf{r}) : l = 1, \dots, K; \mathbf{r} \in \mathcal{D}_Z\}$  via

$$(9) \quad z(\mathbf{r}, t) = \sum_{l=1}^K a_l(t) \psi_l(\mathbf{r}),$$

then linearity of the integral in (2) and reduced rank approximation (6) can induce a reparameterized, reduced-rank teleconnection effect process  $\alpha'(\mathbf{s}, l)$  for patterns  $l = 1, \dots, K$  by

$$(10) \quad \alpha'(\mathbf{s}, l) = \sum_{j=1}^k \alpha(\mathbf{s}, \mathbf{r}_j^*) \int_{\mathcal{D}_Z} \psi_l(\mathbf{r}) h(\mathbf{r}, \mathbf{r}_j^*) d\mathbf{r}.$$

Note that the transformation appears naturally since

$$(11) \quad \begin{aligned} \int_{\mathcal{D}_Z} z(\mathbf{r}, t) \alpha(\mathbf{s}, \mathbf{r}) d\mathbf{r} &= \int_{\mathcal{D}_Z} \sum_{l=1}^K a_l(t) \psi_l(\mathbf{r}) \sum_{j=1}^k h(\mathbf{r}, \mathbf{r}_j^*) \alpha(\mathbf{s}, \mathbf{r}_j^*) d\mathbf{r} \\ &= \sum_{l=1}^K a_l(t) \sum_{j=1}^k \alpha(\mathbf{s}, \mathbf{r}_j^*) \int_{\mathcal{D}_Z} \psi_l(\mathbf{r}) h(\mathbf{r}, \mathbf{r}_j^*) d\mathbf{r} \\ &= \sum_{l=1}^K a_l(t) \alpha'(\mathbf{s}, l). \end{aligned}$$

Principal component decompositions, known as empirical orthogonal functions (EOFs) in climate science, are a special case of (9). EOFs are particularly useful expansions for teleconnection since these transformations meaningfully characterize phenomena that impact global climate (Ashok et al., 2007).

**2.4. Model likelihood.** Using Gaussian processes to specify the RESP model's (1) randomness implies the data likelihood is jointly normal for finite samples with  $n_s$  locations,  $n_r$  remote locations, and  $n_t$  timepoints. Let the column vectors  $\mathbf{Y}_t = [Y(\mathbf{s}_i, t)]_{i=1}^{n_s} \in \mathbb{R}^{n_s}$  and  $\mathbf{z}_t = [z(\mathbf{r}_j, t)]_{j=1}^{n_r} \in \mathbb{R}^{n_r}$ , and the matrix  $X_t \in \mathbb{R}^{n_s \times p}$  with row vectors  $\mathbf{x}(\mathbf{s}_i, t)^T$  for  $i = 1, \dots, n_s$  represent the observed response variables and covariates at time  $t$ ; and let the column vector  $\boldsymbol{\alpha}(\mathbf{s}) = [\alpha(\mathbf{s}, \mathbf{r}_j)]_{j=1}^{n_r} \in \mathbb{R}^{n_r}$  represent the teleconnection coefficients for location  $\mathbf{s}$ . The reduced rank assumption lets us use the Kriging notation from (7) to write  $\boldsymbol{\alpha}(\mathbf{s}) = \mathbf{c}^* R^{*-1} \boldsymbol{\alpha}^*(\mathbf{s})$ . The matrix  $\mathbf{c}^* \in \mathbb{R}^{n_r \times k}$  is built with row vectors  $\mathbf{c}^*(\mathbf{r}_i)^T$  for  $i = 1, \dots, n_r$  that contain the covariances between the teleconnection effect  $\alpha(\mathbf{s}, \mathbf{r}_i)$  and the teleconnection effects at knot locations  $\alpha(\mathbf{s}, \mathbf{r}_j^*), j = 1, \dots, k$ . This yields the data likelihood for  $\mathbf{Y} = [\mathbf{Y}_{t_1}^T \dots \mathbf{Y}_{t_{n_t}}^T]^T \in \mathbb{R}^{n_s n_t}$ , which is given by

$$(12) \quad \mathbf{Y} | \boldsymbol{\beta}, \tilde{\boldsymbol{\alpha}}^*, R^*, \mathbf{c}^*, \Sigma \sim \mathcal{N}(\boldsymbol{\mu}_{\mathbf{Y}}, I_{n_t} \otimes \Sigma)$$

in which

$$\boldsymbol{\mu}_Y = \tilde{\mathbf{X}} (\mathbf{1}_{n_t} \otimes \boldsymbol{\beta}) + \tilde{\mathbf{Z}}^* (\mathbf{1}_{n_t} \otimes \tilde{\boldsymbol{\alpha}}^*)$$

$\otimes$  denotes the Kronecker product,

$\tilde{\mathbf{X}} = \text{diag} \{X_{t_1}, \dots, X_{t_{n_t}}\}$ ,  $\tilde{\mathbf{Z}}^* = \text{diag} \{I_{n_s} \otimes \mathbf{z}_{t_1}^{*T}, \dots, I_{n_s} \otimes \mathbf{z}_{t_{n_t}}^{*T}\}$ ,  $\mathbf{z}_t^{*T} = \mathbf{z}_t^T \mathbf{c}^* R^{*-1} \in \mathbb{R}^{1 \times k}$ ,  $\tilde{\boldsymbol{\alpha}}^* = [\boldsymbol{\alpha}^*(\mathbf{s}_i)]_{i=1}^{n_s} \in \mathbb{R}^{n_s k}$ , and  $\Sigma \in \mathbb{R}^{n_s \times n_s}$  is the local covariance matrix with entries  $\Sigma_{ij} = C_w \{(\mathbf{s}_i, t), (\mathbf{s}_j, t)\}$ . While the covariate matrices  $\tilde{\mathbf{X}} \in \mathbb{R}^{n_s n_t \times p_{nt}}$  and  $\tilde{\mathbf{Z}} \in \mathbb{R}^{n_s n_t \times n_s k_{nt}}$  are block diagonal, we introduce alternate notation in Section 2.5 to make evaluating posterior distributions easier.

Each time-indexed block in the remote effects term  $\tilde{\mathbf{Z}}^* (\mathbf{1}_{n_t} \otimes \tilde{\boldsymbol{\alpha}}^*)$  has the form  $(I_{n_s} \otimes \mathbf{z}_t^{*T}) \tilde{\boldsymbol{\alpha}}^*$ , which helps show how each response  $Y(\mathbf{s}, t)$  at time  $t$  shares the same remote covariates  $\mathbf{z}_t^*$ . Although the remote coefficients  $\alpha(\mathbf{s}, \mathbf{r}^*)$ ,  $\mathbf{s} \in \mathcal{D}_Y$  vary spatially across  $\mathcal{D}_Y$  for a fixed  $\mathbf{r}^* \in \mathcal{D}_Z$ , the RESP model differs from traditional spatially varying coefficient models (cf. [Banerjee, Carlin and Gelfand, 2015](#), Section 9.6) because all of these remote coefficients share the same covariate  $z^*(\mathbf{r}^*, t)$ .

The likelihood (12) changes subtly when reparameterizing the teleconnection effects (2) to interpret them with respect to the spatial basis function transformation defined by (10). The spatial basis function expansion (9) of the remote covariates  $z(\mathbf{r}, t)$  yields the substitution

$$(13) \quad \tilde{\mathbf{Z}}^* (\mathbf{1}_{n_t} \otimes \tilde{\boldsymbol{\alpha}}^*) = \tilde{\mathbf{A}} (\mathbf{1}_{n_t} \otimes \tilde{\boldsymbol{\alpha}}')$$

in the likelihood (12). Where  $\tilde{\mathbf{A}} = \text{diag} \{I_{n_s} \otimes \mathbf{A}_{t_1}^T, \dots, I_{n_s} \otimes \mathbf{A}_{t_{n_t}}^T\}$  and  $\tilde{\boldsymbol{\alpha}}' = (I_{n_s} \otimes W^T \mathbf{c}^* R^{*-1})$ , and  $\tilde{\boldsymbol{\alpha}}^* \in \mathbb{R}^{n_s K}$  where the vector  $\mathbf{A}_t$  and matrix  $W$  form the matrix decomposition of the remote covariate vector  $\mathbf{z}_t$  when expanded by spatial basis functions  $\mathbf{z}_t = W \mathbf{A}_t$ . The column vector  $\mathbf{A}_t = [a_l(t)]_{l=1, \dots, K} \in \mathbb{R}^K$  contains the weights at time  $t$  for the basis functions  $\{\psi_l(\mathbf{r}) : l = 1, \dots, K\}$ , which are stored in the basis function matrix  $W \in \mathbb{R}^{n_r \times K}$  with entries  $W_{jl} = \psi_l(\mathbf{r}_j)$ .

**2.5. Bayesian implementation.** We adopt a hierarchical Bayesian framework and use a hybrid Gibbs sampler for inference for the RESP model (1) using the likelihood (12). The Bayesian framework allows estimates for the transformed teleconnection effects (10) to be computed directly from posterior samples of  $\tilde{\boldsymbol{\alpha}}^*$  by using the definition for  $\tilde{\boldsymbol{\alpha}}'$  specified after (13) to appropriately transform the sampled teleconnection effects  $\tilde{\boldsymbol{\alpha}}^*$ . Full details for priors and full conditional posterior distributions provided in Supplement A ??.

Studying the posterior distribution for the remote coefficients  $\tilde{\boldsymbol{\alpha}}^*$  helps build intuition for their estimates. The Gaussian process assumption and separable covariance (4) imply the remote coefficients have prior distribution

$$(14) \quad \tilde{\boldsymbol{\alpha}}^* | \Sigma, R^* \sim \mathcal{N}(\mathbf{0}, \Sigma \otimes R^*).$$

The full conditional posterior distribution for  $\tilde{\boldsymbol{\alpha}}^*$  is

$$(15) \quad \tilde{\boldsymbol{\alpha}}^* | \cdot \sim \mathcal{N}(\boldsymbol{\mu}_{\tilde{\boldsymbol{\alpha}}^* | \cdot}, \Sigma_{\tilde{\boldsymbol{\alpha}}^* | \cdot}),$$

where “ $\cdot$ ” represents conditioning on all remaining unknown quantities and

$$\begin{aligned} \boldsymbol{\mu}_{\tilde{\boldsymbol{\alpha}}^* | \cdot} &= \sum_{t \in \mathcal{T}} \left\{ (\mathbf{Y}_t - \mathbf{X}_t \boldsymbol{\beta}) \otimes \left( R^{*-1} + \mathbf{Z}^* \mathbf{Z}^{*T} \right)^{-1} \mathbf{z}_t^* \right\}, \\ \Sigma_{\tilde{\boldsymbol{\alpha}}^* | \cdot} &= \Sigma \otimes \left( R^{*-1} + \mathbf{Z}^* \mathbf{Z}^{*T} \right)^{-1}, \end{aligned}$$

and the matrix  $\mathbf{Z}^* \in \mathbb{R}^{k \times n_t}$  with column vectors  $\mathbf{z}_{t_i}^* \in \mathbb{R}^k$  for  $i = 1, \dots, n_t$  is a dense matrix that contains the remote covariates.

The Kronecker structure of  $\boldsymbol{\mu}_{\tilde{\boldsymbol{\alpha}}^* | \cdot}$  and  $\Sigma_{\tilde{\boldsymbol{\alpha}}^* | \cdot}$  makes it easy to study the posterior distribution for the vector of remote coefficients associated with one spatial location  $\boldsymbol{\alpha}^*(\mathbf{s}) = [\alpha(\mathbf{s}, \mathbf{r}_j^*)]_{j=1}^k \in \mathbb{R}^k$ . Recalling that  $\tilde{\boldsymbol{\alpha}}^* = [\boldsymbol{\alpha}^*(\mathbf{s}_i)]_{i=1}^{n_s} \in \mathbb{R}^{n_s k}$  and exploiting the multivariate normal distribution's marginal distribution properties implies

$$(16) \quad \boldsymbol{\alpha}^*(\mathbf{s}) | \cdot \sim \mathcal{N}(\boldsymbol{\mu}_{\boldsymbol{\alpha}^*(\mathbf{s}) | \cdot}, \Sigma_{\boldsymbol{\alpha}^*(\mathbf{s}) | \cdot})$$

in which

$$(17) \quad \boldsymbol{\mu}_{\boldsymbol{\alpha}^*(\mathbf{s}) | \cdot} = \sum_{t \in \mathcal{T}} \boldsymbol{\Psi} \left( \mathbf{Y}(\mathbf{s}, t) - \mathbf{x}(\mathbf{s}, t)^T \boldsymbol{\beta} \right) \mathbf{z}_t^*,$$

$$(18) \quad \Sigma_{\boldsymbol{\alpha}^*(\mathbf{s}) | \cdot} = \Sigma_{\mathbf{s}, \mathbf{s}} \boldsymbol{\Psi},$$

$\Sigma_{\mathbf{s}, \mathbf{s}}$  is the  $s^{th}$  diagonal entry in  $\Sigma$ , and

$$\boldsymbol{\Psi} = \left( R^{*-1} + \mathbf{Z}^* \mathbf{Z}^{*T} \right)^{-1}.$$

With manipulations detailed in Supplement A ??, this distributional form is equivalent to the posterior distribution of a Bayesian linear regression of the local residuals over time  $\left[ \mathbf{Y}(\mathbf{s}, t) - \mathbf{x}(\mathbf{s}, t)^T \boldsymbol{\beta} \right]_{t=1}^{n_t} \in \mathbb{R}^{n_t}$  onto the remote covariates  $\mathbf{Z}^{*T}$  when using a prior mean of  $\mathbf{0}$  and prior covariance

matrix  $\Sigma_{\mathbf{s},\mathbf{s}} R^*$  for  $\boldsymbol{\alpha}^*(\mathbf{s})$ . This suggests that patterns in maps of posterior means of  $\tilde{\boldsymbol{\alpha}}^*$  can resemble patterns in maps that show pointwise correlations  $\text{Cor}_t(z^*(\mathbf{r}^*, t), Y(\mathbf{s}, t))$  between specific remote covariates  $\{z^*(\mathbf{r}^*, t) : t \in \mathcal{T}\}$  and local responses  $\{Y(\mathbf{s}, t) : t \in \mathcal{T}\}$ . Similar manipulations show that patterns in maps of posterior means of the reparameterized teleconnection effects  $\tilde{\boldsymbol{\alpha}}'$  can resemble patterns in maps that show pointwise correlations  $\text{Cor}_t(a_k(t), Y(\mathbf{s}, t))$  between specific spatial basis function coefficients  $\{a_k(t) : t \in \mathcal{T}\}$  and local responses  $\{Y(\mathbf{s}, t) : t \in \mathcal{T}\}$ .

**2.6. Computational approach for conducting inference on remote coefficients.** We use standard hierarchical Bayesian spatial modeling techniques to draw inference on  $\tilde{\boldsymbol{\alpha}}^*$  through composition sampling (Banerjee, Carlin and Gelfand, 2015, p. 126). Composition sampling generates a posterior sample  $\{\tilde{\boldsymbol{\alpha}}^{*(1)}, \dots, \tilde{\boldsymbol{\alpha}}^{*(G)}\}$  for  $\tilde{\boldsymbol{\alpha}}^*$  by using the full conditional posterior distribution (15) for  $\tilde{\boldsymbol{\alpha}}^*$  with a posterior sample of the model parameters  $\boldsymbol{\beta}$ ,  $\boldsymbol{\theta}_w$ ,  $\boldsymbol{\theta}_\alpha$ , and  $\sigma_\varepsilon^2$ . Since composition samples  $\tilde{\boldsymbol{\alpha}}^{*(i)}$  are independent given the posterior parameter samples, the composition samples may be drawn in parallel to reduce the computation time. Drawing inference on  $\tilde{\boldsymbol{\alpha}}^*$  also requires computational techniques to reduce memory demands.

The composition sample for  $\tilde{\boldsymbol{\alpha}}^*$  requires storing  $n_s \times k \times G$  floating point numbers. Even for moderately sized studies with  $n_s = 200$ ,  $k = 30$ , and  $G = 20,000$ , the composition sample requires 915MB of memory. Although this demand increases linearly in  $k$ ,  $n_s$ , and  $G$ , it quickly becomes burdensome for typical personal computers. We therefore estimate  $\tilde{\boldsymbol{\alpha}}^*$  using the normal approximation to the posterior. The normal approximation only requires the composition sample's mean  $\hat{\boldsymbol{\mu}}_{\tilde{\boldsymbol{\alpha}}|\mathbf{Y}} = \frac{1}{G} \sum_{g=1}^G \tilde{\boldsymbol{\alpha}}^{*(g)}$  and covariance matrix  $\hat{\Sigma}_{\tilde{\boldsymbol{\alpha}}|\mathbf{Y}} = \frac{1}{G-1} \sum_{g=1}^G (\tilde{\boldsymbol{\alpha}}^{*(g)} - \hat{\boldsymbol{\mu}}_{\tilde{\boldsymbol{\alpha}}|\mathbf{Y}}) (\tilde{\boldsymbol{\alpha}}^{*(g)} - \hat{\boldsymbol{\mu}}_{\tilde{\boldsymbol{\alpha}}|\mathbf{Y}})^T$ . These objects require storing  $(n_s \times k)(n_s \times k + 3)/2$  floating point numbers, which can dramatically reduce memory requirements when  $G > (n_s \times k + 3)/2$ .

We use strategies from Pébay (2008) to facilitate computing these summary objects with minimal memory requirements. We use partitions of the composition samples and compute  $\hat{\boldsymbol{\mu}}_{\tilde{\boldsymbol{\alpha}}|\mathbf{Y}}$  and  $\hat{\Sigma}_{\tilde{\boldsymbol{\alpha}}|\mathbf{Y}}$  in a streaming fashion, which allows estimation of  $p(\tilde{\boldsymbol{\alpha}}^*|\mathbf{Y})$  in parallel and with minimal memory requirements (Pébay, 2008, eqs. 1.1, 1.3, 3.11, & 3.12). These benefits are achieved by recognizing, for example, that a running estimate of  $\hat{\boldsymbol{\mu}}_{\tilde{\boldsymbol{\alpha}}|\mathbf{Y}}$  based on  $\{\tilde{\boldsymbol{\alpha}}^{*(1)}, \dots, \tilde{\boldsymbol{\alpha}}^{*(g)}\}$  is easy to update when the next composition sample  $\tilde{\boldsymbol{\alpha}}^{*(g+1)}$  is drawn, and that the updating equations yield  $\hat{\boldsymbol{\mu}}_{\tilde{\boldsymbol{\alpha}}|\mathbf{Y}}$  once all  $G$  composition samples are processed.

**2.7. Model assessment.** We use ranked probability scores (RPS) to compare how well the RESP model and standard statistical downscaling methods predict ordered, discrete categorical summaries of precipitation. The RPS compares probabilistic predictions of ordinal variables, giving lower scores to models that generate predictive distributions that better match the true distribution (Gneiting and Raftery, 2007). We present RPS results in Section 3.4.2. We also use the Heidke skill score to assess predictive performance. Heidke skill scores are commonly used in climate science to measure a model’s misclassification rate for categorical point predictions (von Storch and Zwiers, 1999, Section 18.1). Heidke skill scores and variance inflation factors (VIFs) are presented in Supplement A, ?? along with formulas and more details for all of these measures.

**3. Colorado winter precipitation.** We demonstrate that the RESP model (1) improves downscaled predictions of Colorado winter precipitation. We use a leave-one-out cross-validation study to compare the RESP model to more common statistical downscaling methods. We introduce the study data (Section 3.1), describe the comparison methods (Section 3.2), and present results (Section 3.4).

**3.1. Data.** This study uses the ERA-Interim reanalysis dataset to provide sea surface temperatures and local covariates (Dee et al., 2011). The response, precipitation, comes from the PRISM dataset (Daly et al., 2008). We limit our study period to 1981 through 2013 since earlier records of large scale climate are less complete. Both datasets are reanalysis products, which are necessary because working directly with observations can be challenging since data may be from various sources and are often spatially sparse and temporally incomplete. As such, reanalysis products use statistical techniques and physical relationships to reproduce consistent datasets at regular, gridded locations with complete records.

This study uses data averaged over the boreal winter months (December, January, February) since Northern Hemisphere teleconnections are often strongest in winter (Nigam and Baxter, 2015). We simplify the demonstration using spatially-referenced variables average surface air temperature over Colorado ( $T$ ) and average Pacific Ocean sea surface temperatures ( $SST$ ) between  $120^{\circ}\text{E}$ – $70^{\circ}\text{W}$  and  $20^{\circ}\text{S}$ – $60^{\circ}\text{N}$  to predict the spatial response, average winter precipitation in Colorado ( $P$ ). We also standardize all data to remove the impact of orographic and other location-based effects by removing the pointwise mean from all data and scaling data to have unit variance. We standardize our data before conducting the leave-one-out cross-validation study so all of the testing and training data are comparable. Thus, our data

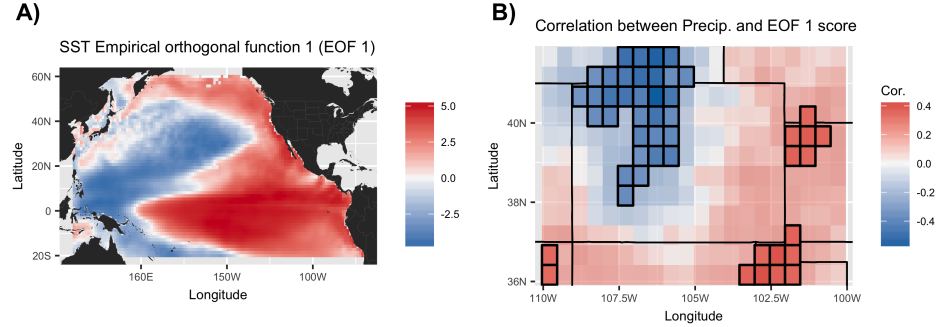


FIG 2. *Exploratory analysis plots.* A) The first empirical orthogonal function (EOF)  $\psi_1 : \mathcal{D}_Y \rightarrow \mathbb{R}$  for standardized anomalies of Pacific Ocean sea surface temperatures is an indicator of El Niño events, during which sea surface temperatures are anomalously warm in the central and eastern Pacific Ocean tropics but anomalously cool in the western tropics (Ashok et al., 2007). EOF 1 accounts for 30% of the variability in sea surface temperatures. B) Pointwise correlations  $\text{Cor}_t(P(\mathbf{s}, t), a_1(t))$  between Colorado precipitation  $P(\mathbf{s}, t)$  and the EOF 1 score  $a_1(t)$  suggest northern and western/central Colorado tends to receive less precipitation than average during El Niño events while eastern Colorado tends to receive more precipitation. Significant correlations (naive independent  $p$ -value  $< .05$ ) are highlighted, while non-significant correlations are faded slightly.

are standardized climate anomalies that, for example, represent the number of standard deviations  $P(\mathbf{s}, t)$  is above or below the time-averaged value  $E[t] P(\mathbf{s}, t)$  at location  $\mathbf{s}$ . The data are also spatially aggregated so that 240 42km-resolution grid cells cover Colorado and 5,252 78km-resolution grid cells cover the Pacific Ocean, and distances between grid cells are measured with great-circle distances.

We use Pacific Ocean sea surface temperature to capture how the ocean influences Colorado precipitation through the El Niño–Southern Oscillation (ENSO) teleconnection (Lukas et al., 2014, Figure 2.4). The ENSO teleconnection is characterized by sea surface temperatures that are anomalously warm in the central and eastern Pacific Ocean tropics but anomalously cool in the western tropics. The first empirical orthogonal function (EOF; i.e., principal component)  $\psi_1 : \mathcal{D}_Y \rightarrow \mathbb{R}$  for Pacific Ocean sea surface temperature anomalies illustrates this pattern (Figure 2). Pointwise correlations  $\text{Cor}_t(a_1(t), P(\mathbf{s}, t))$  between the ENSO teleconnection’s strength  $a_1(t)$  and Colorado precipitation  $P(\mathbf{s}, t)$  provide standard evidence for teleconnection, suggesting northern and western/central Colorado tend to receive significantly less precipitation than average during ENSO events, which are periods of strong El Niño activity, while plains regions bordering eastern

Colorado tend to receive significantly more precipitation than average (Figure 2). Note, however, that this analysis does not account for spatial correlation and thus may require correction.

**3.2. Comparison models.** We compare the RESP model to several common methods for statistical downscaling and prediction, such as a hybrid local and non-local regression using the El-Niño–Southern Oscillation teleconnection (ENSO-T) (van den Dool, 2007, Sections 8.4, 8.5), canonical correlation analysis (CCA) (von Storch and Zwiers, 1999, Chapter 14), and a baseline climatological reference prediction (CLIM) (van den Dool, 2007, Section 8.1).

**3.2.1. Hybrid local and non-local regression (ENSO-T).** Pointwise regression models are commonly used to downscale climate data. The ENSO-T model predicts precipitation  $P(\mathbf{s}, t_0)$  at a location  $\mathbf{s}$  and new timepoint  $t_0$  by applying a regression of training data  $P(\mathbf{s}, t)$  onto local surface air temperature  $T(\mathbf{s}, t)$  and the score  $a_1(t)$  for the first sea surface temperature EOF  $\psi_1 : \mathcal{D}_Y \rightarrow \mathbb{R}$ . The ENSO-T downscaler provides a comparison model that accounts for both local and remote effects, but not spatial dependence.

**3.2.2. Canonical correlation analysis (CCA).** Canonical correlation analysis uses the empirical correlation structure of sea surface temperature  $SST$  and precipitation  $P$  vectors to linearly map these variables to a space in which the transformed vectors are maximally correlated (von Storch and Zwiers, 1999, Chapter 14). This mapping may be used in a multivariate regression context with sea surface temperatures at new timepoints to predict precipitation. The mapping is often developed with some amount of smoothing by removing higher order EOFs from the data. We retain 16 EOFs in our use of CCA since this lets us capture 90% of the variability in the predictors  $SST$  and predictand  $P$ . The CCA downscaler provides a comparison model that only accounts for remote effects and indirectly accounts for spatial dependence.

**3.2.3. Climatological reference (CLIM).** Climatologists use the unconditional distribution of precipitation  $P(\mathbf{s}, t)$  at a location  $\mathbf{s}$ . When no other information is available, the average value of precipitation  $E_t[P(\mathbf{s}, t)]$  is used as a climatological point prediction for precipitation, and the empirical distribution is used for probabilistic predictions. The CLIM downscaler provides a baseline comparison model that does not account for spatial dependence, local, or remote effects.

**3.3. RESP model and prior specification.** In the RESP model (1), we specify a linear relationship between the local covariate  $T$  and response  $P$  so that  $\beta$  in (1) has intercept  $\beta_0$  and slope  $\beta_T$  components  $\beta = (\beta_0, \beta_T)^T$ . For the RESP model's remote coefficients, knots are placed at 42 locations that are roughly evenly spaced across the Pacific Ocean and along coastal locations (Supplement A, ??). While knot selection can be problematic, Banerjee et al. (2008) find that reasonably dense, regularly spaced grids can yield good results. Since the ENSO teleconnection is scientifically meaningful, we will interpret the transformed teleconnection effects  $\alpha'(\mathbf{s}, 1)$  from (10), which are associated with ENSO through its connection to the first empirical orthogonal function (EOF) of sea surface temperature anomalies  $\psi_1 : \mathcal{D}_Y \rightarrow \mathbb{R}$ .

We adopt a combination of weakly informative and non-informative prior distributions. A dispersed normal prior is used for the fixed effects  $\beta \sim \mathcal{N}(\mathbf{0}, 10I)$ . We use  $\sigma_w^2 \sim IG(2, 30)$ ,  $\sigma_\alpha^2 \sim IG(2, 1)$ ,  $\sigma_\varepsilon^2 \sim IG(2, 1)$ ,  $\rho_w \sim U(1, 600)$ , and  $\rho_\alpha \sim U(1, 600)$ . The Matérn covariance smoothness parameters (5) are fixed at  $\nu_w = 2$  and  $\nu_\alpha = 1.76$ , which were determined by inspecting variograms for the local and remote data.

**3.4. Results.** Model results are based on 20,000 samples from the posterior distribution after a burn in period of 1,000 samples. Convergence was assessed by examining traceplots, autocorrelation plots, and effective sample sizes in addition to comparing results from multiple runs with randomly initialized parameters. Model adequacy was assessed using residual and qq-normal plots. These diagnostics suggest there are no serious violations of the convergence and distributional assumptions.

**3.4.1. Inference.** Parameter estimates for the RESP model yield reasonable scientific interpretations (Table 1). The sign of the regression coefficient  $\beta_T$  for the temperature covariate  $T$  is consistent with physical processes that influence precipitation (Daly et al., 2008). The local covariance range parameter  $\rho_w$  implies the dependence between locations  $\mathbf{s} \in \mathcal{D}_Y$  has an effective range between 190km and 200km, which is the distance between locations beyond which the Matérn correlation (5) is small ( $\leq .05$ ). This length scale is in the size range of mesoscale weather processes that produce precipitation (Parker, 2015).

The remote covariance range parameter  $\rho_\alpha$  suggests the dependence between remote coefficients  $\alpha(\mathbf{s}, \mathbf{r})$  and  $\alpha(\mathbf{s}, \mathbf{r}')$  has an effective range between 5km and 55km. The small effective range suggests the remote coefficients  $\alpha(\mathbf{s}, \mathbf{r})$  are effectively independent since the sea surface temperature data is measured on 78km-resolution grid cells. The transformed remote coefficients

TABLE 1

Posterior mean estimates and 95% highest posterior density (HPD) intervals for the RESP model's parameters, which include an intercept  $\beta_0$  and temperature effect  $\beta_T$  on the mean response (see equation (1)), and covariance scale  $\sigma^2$  and range  $\rho$  parameters for the local  $w$  and remote  $\alpha$  spatial dependence and nugget effect  $\varepsilon$  (see (3) and (4)). The smoothness parameters  $\nu_w$  and  $\nu_\alpha$  were fixed (Section 3.3).

		Posterior mean	95% HPD
Local effects	$\beta_0$	-0.000	(-0.062, 0.063)
	$\beta_T$	-0.206	(-0.26, -0.154)
Covariance	$\sigma_w^2$	0.357	(0.336, 0.379)
	$\sigma_\alpha^2$	0.004	(0.003, 0.005)
	$\sigma_\varepsilon^2$	0.031	(0.029, 0.033)
	$\rho_w$	39.563	(38.224, 40.778)
	$\rho_\alpha$	6.109	(1.464, 10.168)

$\alpha'(\mathbf{s}, l)$ , however, are still interpretable since they are defined with respect to the sea surface temperature anomaly EOFs  $\psi_l : \mathcal{D}_Y \rightarrow \mathbb{R}$ , which are not affected by the small remote range parameter  $\rho_\alpha$ . The model's implicit suggestion to study the transformed remote coefficients  $\alpha'(\mathbf{s}, l)$  rather than the original remote coefficients  $\alpha(\mathbf{s}, \mathbf{r})$  is consistent with the way teleconnection phenomena work: specific configurations of sea surface temperatures, rather than individual points, are oftentimes most scientifically meaningful. Posterior estimates for the transformed remote effects  $\{\alpha'(\mathbf{s}, 1) : \mathbf{s} \in \mathcal{D}_Y\}$  associated with  $\psi_1 : \mathcal{D}_Y \rightarrow \mathbb{R}$  (Figure 3) closely match the exploratory pointwise correlations between  $P(\mathbf{s}, t)$  and  $a_1(t)$  found in the exploratory plot (Figure 2), indicating the RESP model (1) is capturing known Colorado teleconnections. Since these estimates are computed using a spatial model, however, their pointwise significance properly accounts for spatial correlation between locations. This is an improvement over existing methods (e.g., see Figure 2).

**3.4.2. Prediction.** Climate scientists often evaluate seasonal precipitation predictions, which may be derived through downscaling, using categorical predictions of whether precipitation is expected to be “above average”, “near average”, or “below average” at each location. Categorical predictions are favored because it is inherently difficult to develop more precise climate predictions at seasonal and longer time scales (Mason, 2012; van den Dool, 2007, Section 9.6). Category cutpoints are determined for each location  $\mathbf{s}$  using the empirical terciles of precipitation  $P(\mathbf{s}, t)$  over the leave-one-out training data.

We use the ranked probability score to compare categorical probabilistic

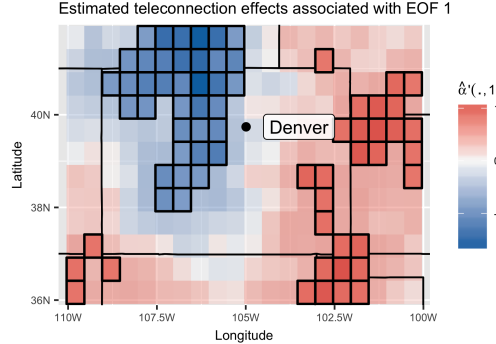


FIG 3. Estimated teleconnection effects  $\hat{\alpha}'(s, 1)$  for EOF 1  $\psi_1 : \mathcal{D}_Y \rightarrow \mathbb{R}$ . The overall patterns yield similar interpretations as those made with the [Figure 2](#) exploratory plots, however, the RESP model uses spatial dependence to enlarge the regions in which evidence exists for significant teleconnection. Significant teleconnection effects, as determined using 95% highest posterior density intervals, are highlighted.

predictions between the RESP, ENSO-T, CCA, and CLIM models (Section 2.7, Section 3.2). Results using the Heidke skill score for categorical point predictions are similar and presented in Supplement A, ???. The predictive distributions for the RESP, ENSO-T, and CLIM models are continuous, but easily discretized with respect to category cutpoints that are empirically determined from the leave-one-out training data. However, the CCA model only yields point predictions since predictive uncertainties are difficult to obtain. Thus, the CCA’s discretized predictive distribution is defined by a point mass on the category that matches the “above average”, “near average”, or “below average” range in which the point prediction lies.

The RESP model (1) frequently yields better probabilistic predictions than the comparison models [Figure 4](#)). While the ENSO-T downscaler is attractive for its simplicity, the comparisons show its performance is weaker and more variable than the RESP model. The RESP model’s improvement is likely due to regularization induced by accounting for spatial dependence. The CCA RPS values are inflated because the model does not produce true probabilistic predictions, thus highlighting deeper advantages of the RESP model.

**4. Discussion.** Since there is great uncertainty in GCM’s prediction of future precipitation, statistical downscaling methods have been widely used in regional climate change studies. The RESP model (1) developed here marks an improvement in statistical downscaling and extends geostatistical models to incorporate the effect of both local and remote covariates

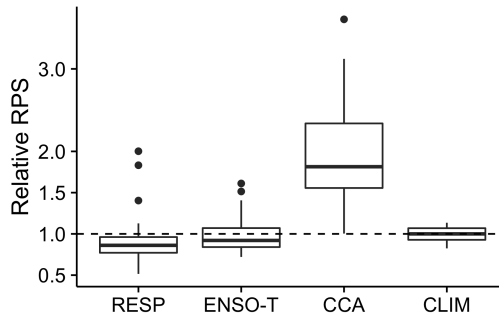


FIG 4. Comparison of Ranked probability scores (RPS) for probabilistic categorical predictions on the leave-one-out test datasets for the RESP, ENSO-T, CCA, and CLIM models. RPS scores are reported relative to the median RPS for the CLIM reference model's unconditional predictions. The RESP model generally has better (i.e., lower) and slightly less variable skill than the comparison models.

on spatially correlated responses, like precipitation. As such, although our model is developed and validated on historical data, in a regional climate change application, it could be used with GCM predictions of surface temperatures and large-scale patterns to infer predictions for precipitation. We demonstrate in a cross-validation study that the RESP model tends to make better predictions for precipitation than standard downscaling models that, individually, only account for some of the features of the RESP model. The RESP model also improves upon standard methods for estimating teleconnections by explicitly modeling spatial dependence between local and remote covariates, thus providing statistically valid inference.

The RESP model is defined for continuous response variables, but could be extended to a generalized linear model (GLM) structure. While it is a standard approach to model precipitation data—which are notoriously challenging to estimate—with continuous distributions and evaluate model fit using terciles, a GLM structure could also be used to directly model the categorical response. A GLM structure could also allow fitting count data, like the seasonal number of large rain events, which is also important for many sectors of society and ecological systems.

Equipping the RESP model with nonstationary covariance structures or spatially varying coefficients for local effects may also improve fit. In particular, nonstationary covariances could allow the remote coefficients to vary temporally. This extension may be relevant because [Mason and Goddard \(2001\)](#) find that teleconnection effects can vary across seasons. As in [Choi et al. \(2015\)](#), however, changes over time may be difficult to detect

because the effects tend to be weak. Other generalizations to the RESP model's covariance structure may also greatly increase computational demands. The existing model induces a separable covariance structure that makes estimation efficient.

Increased computational demands associated with generalizing the RESP model could be offset by applying various approximate spatial modeling techniques to the local or remote covariance matrices. Although we used a predictive process approximation to model the remote coefficients, predictive process approximations can also be applied to the local covariance matrix. Other options include, but are not limited to, hierarchical nearest neighbor models (Datta et al., 2016), covariance tapering (Furrer, Genton and Nychka, 2006), and multiresolution covariance models (Katzfuss, 2016). These techniques could also be used to apply the RESP model to higher resolution datasets.

There is potential for more diverse application of the model since notions of teleconnection exist in other fields, like ecology (Brierley et al., 1999) and human geography (Seto et al., 2012). Additionally, the model's general introduction in Section 2 as a spatial regression problem highlights a class of spatial problems that standard geostatistical models do not consider. The model addresses spatial problems in which dependence does not follow a central spatial statistics assumption that spatial processes at distant locations are effectively independent. While the RESP model requires that the response and local and remote covariates be defined on disjoint spatial domains, it suggests a broader class of related problems in which overlapping domains characterize dependence between distant locations, or in which appropriate disjoint domains are not known a priori and need to be estimated during model fitting. This problem description is reminiscent of general covariance or graphical model structure estimation problems, which may provide possible directions for future spatial statistics research topics.

**Acknowledgements.** We thank Tilmann Gneiting, Editor-In-Chief of AOAS, for his suggestions. We also express our gratitude to Professor Michael Stein and Dr. Mikael Kuusela for discussions that helped enrich the interpretation of this work. This material is based upon work supported by the National Science Foundation under Grant Number (NSF AGS - 1419558 and DMS-1106862). Any opinions, findings, and conclusions or recommendations expressed in this material are those of the authors and do not necessarily reflect the views of the National Science Foundation.

## SUPPLEMENTARY MATERIAL

**Supplement A: Supporting computations and figures**

(doi: [COMPLETED BY THE TYPESETTER](#); .pdf). We provide details used to derive several theoretical and computational results as well as some supporting figures for the study of Colorado precipitation.

**References.**

ADLER, R. J. and TAYLOR, J. E. (2007). *Random Fields and Geometry*. Springer Science + Business Media, LLC, New York.

ASHOK, K., BEHERA, S. K., RAO, S. A., WENG, H. and YAMAGATA, T. (2007). El Nino Modoki and its possible teleconnection. *Journal of Geophysical Research* **112** 1–27.

ASSUNÇÃO, R. and KRAINSKI, E. (2009). Neighborhood Dependence in Bayesian Spatial Models. *Biometrical Journal* **51** 851–869.

BANERJEE, S., CARLIN, B. P. and GELFAND, A. E. (2015). *Hierarchical Modeling and Analysis for Spatial Data*, 2 ed. CRC Press, Boca Raton, FL.

BANERJEE, S., GELFAND, A. E., FINLEY, A. O. and SANG, H. (2008). Gaussian predictive process models for large spatial data sets. *Journal of the Royal Statistical Society. Series B: Statistical Methodology* **70** 825–848.

BRIERLEY, A. S., DEMER, D. A., WATKINS, J. L. and HEWITT, R. P. (1999). Concordance of interannual fluctuations in acoustically estimated densities of Antarctic krill around South Georgia and Elephant Island: Biological evidence of same-year teleconnections across the Scotia Sea. *Marine Biology* **134** 675–681.

BRUYERE, C. L., HOLLAND, G. J. and TOWLER, E. (2012). Investigating the Use of a Genesis Potential Index for Tropical Cyclones in the North Atlantic Basin. *Journal of Climate* **25** 8611–8626.

CHOI, I., LI, B., ZHANG, H. and LI, Y. (2015). Modelling space-time varying ENSO teleconnections to droughts in North America. *Stat* **4** 140–156.

DALY, C., HALBLEIB, M., SMITH, J. I., GIBSON, W. P., DOGGETT, M. K., TAYLOR, G. H., CURTIS, J. and PASTERIS, P. P. (2008). Physiographically sensitive mapping of climatological temperature and precipitation across the conterminous United States. *International Journal of Climatology* **28** 2031–2064.

DATTA, A., BANERJEE, S., FINLEY, A. and GELFAND, A. (2016). Hierarchical Nearest-Neighbor Gaussian Process Models for Large Geostatistical Datasets. *Journal of the American Statistical Association* **111** 800–812.

DEE, D. P., UPPALA, S. M., SIMMONS, A. J., BERRISFORD, P., POLI, P., KOBAYASHI, S., ANDRAE, U., BALMASEDA, M. A., BALSAMO, G., BAUER, P., BECHTOLD, P., BELJAARS, A. C. M., VAN DE BERG, L., BIDLOT, J., BORMANN, N., DELSOL, C., DRAGANI, R., FUENTES, M., GEER, A. J., HAIMBERGER, L., HEALY, S. B., HERSBACH, H., HÓLM, E. V., ISAKSEN, L., KÅLLBERG, P., KÖHLER, M., MATRICARDI, M., McNALLY, A. P., MONGE-SANZ, B. M., MORCRETTE, J. J., PARK, B. K., PEUBEY, C., DE ROSNAY, P., TAVOLATO, C., THÉPAUT, J. N. and VITART, F. (2011). The ERA-Interim reanalysis: Configuration and performance of the data assimilation system. *Quarterly Journal of the Royal Meteorological Society* **137** 553–597.

DESER, C., PHILLIPS, A., BOURDETTE, V. and TENG, H. (2012). Uncertainty in climate change projections : the role of internal variability. *Climate Dynamics* **38** 527–546.

FLATO, G., MAROTZKE, J., ABIODUN, B., BRACONNOT, P., CHAN CHOU, S., COLLINS, W., COX, P., DRIOUECH, F., EMORI, S., EYRING, V., FOREST, C., GLECKLER, P., GUILYARDI, E., JAKOB, C., KATTSOV, V., REASON, C. and RUMMUKAINEN, M.

(2013). Evaluation of Climate Models 9. In *Climate Change 2013: The Physical Science Basis. Contribution of Working Group I to the Fifth Assessment Report of the Intergovernmental Panel on Climate Change* 9, 741–882. Cambridge University Press, Cambridge, United Kingdom.

FOWLER, H. J., BLENKINSOP, S. and TEBALDI, C. (2007). Linking climate change modelling to impacts studies : recent advances in downscaling techniques for hydrological. *International Journal of Climatology* **27** 1547–1578.

FURRER, R., GENTON, M. G. and NYCHKA, D. (2006). Covariance Tapering for Interpolation of Large Spatial Datasets. *Journal of Computational and Graphical Statistics* **15** 502–523.

GNEITING, T. and RAFTERY, A. E. (2007). Strictly Proper Scoring Rules, Prediction, and Estimation. *Journal of the American Statistical Association* **102** 359–378.

GODDARD, L., MASON, S. J., ZEBIAK, S. E., ROPELEWSKI, C. F., BASHER, R. and CANE, M. A. (2001). Current approaches to seasonal-to-interannual climate predictions. *International Journal of Climatology* **21** 1111–1152.

HAWKINS, E. and SUTTON, R. (2010). The potential to narrow uncertainty in projections of regional precipitation change. *Climate Dynamics* **37** 407–418.

KATZFUSS, M. (2016). A multi-resolution approximation for massive spatial datasets. *Journal of the American Statistical Association* **112** 201–214.

LUKAS, J., BARSUGLI, J., DOESKEN, N., RANGWALA, I. and WOLTER, K. (2014). *Climate Change in Colorado*, Second ed. ed. University of Colorado Boulder.

MARAUN, D., WETTERHALL, F., CHANDLER, R. E., KENDON, E. J., WIDMANN, M., BRIENEN, S., RUST, H. W., SAUTER, T., THEMESSL, M., VENEMA, V. K. C., CHUN, K. P., GOODESS, C. M., JONES, R. G., ONOF, C., VRAC, M. and THIELE-EICH, I. (2010). Precipitation downscaling under climate change: Recent developments to bridge the gap between dynamical models and the end user. *Reviews of Geophysics* **48**.

MASON, S. J. (2012). Seasonal and longer-range forecasts. In *Forecast Verification: A Practitioner's Guide in Atmospheric Science* second edi ed. (I. T. Jolliffe and D. B. Stephenson, eds.) 11, 204–220. John Wiley & Sons, Ltd., Oxford.

MASON, S. J. and GODDARD, L. (2001). Probabilistic precipitation anomalies associated with ENSO. *Bulletin of the American Meteorological Society* **82** 619–638.

MONTRY, D. (1997). Linear Relation of Central and Eastern North American Precipitation to Tropical Pacific Sea Surface Temperature Anomalies. *Journal of Climate* **10** 541–558.

MONTRY, D., RICHMAN, M. B. and LAMB, P. J. (1998). Observed Nonlinearities of Monthly Teleconnections between Tropical Pacific Sea Surface Temperature Anomalies and Central and Eastern North American Precipitation. *Journal of Climate* **11** 1812–1835.

NIGAM, S. and BAXTER, S. (2015). Teleconnections. In *Encyclopedia of Atmospheric Sciences 2nd Edition*, 2 ed. **3** 90–109. Elsevier Ltd.

PARKER, D. J. (2015). Mesoscale Meteorology. In *Encyclopedia of Atmospheric Sciences 2nd Edition*, **3** 316–322. Elsevier Ltd.

PÉBAY, P. (2008). Formulas for Robust, One-Pass Parallel Computation of Covariances and Arbitrary-Order Statistical Moments. *Sandia Report SAND2008-6212, Sandia National Laboratories* **94**.

REICH, B. J., HODGES, J. S. and ZADNIK, V. (2006). Effects of residual smoothing on the posterior of the fixed effects in disease-mapping models. *Biometrics* **62** 1197–1206.

SETO, K. C., REENBERG, A., BOONE, C. G., FRAGKIAS, M., HAASE, D., LANGANKE, T., MARCOTULLIO, P., MUNROE, D. K., OLAH, B. and SIMON, D. (2012). Urban land

teleconnections and sustainability. *Proceedings of the National Academy of Sciences* **109** 7687–7692.

TIGNOR, M., ALLEN, S., BOSCHUNG, J., A, N., Y, X., BEX, V. and PM, M. (2013). Climate change 2013: The Physical Science Basis. In *Contribution of working group I to the fifth assessment report of the Intergovernmental Panel on Climate Change*. Cambridge University Press, Cambridge, United Kingdom.

TING, M. F. and WANG, H. (1997). Summertime U.S. precipitation variability and its Relation to Pacific Sea Surface Temperature. *Journal of Climate* **10** 1853–1873.

TOWLER, E., PAIMAZUMDER, D. and HOLLAND, G. (2016). A framework for investigating large-scale patterns as an alternative to precipitation for downscaling to local drought. *Climate Dynamics* 1–12.

VAN DEN DOOL, H. (2007). *Empirical Methods in Short-Term Climate Predictions*. Oxford University Press, Oxford.

VON STORCH, H. and ZWIERS, F. W. (1999). *Statistical Analysis in Climate Research*. Cambridge University Press, Cambridge.

WALL, M. M. (2004). A close look at the spatial structure implied by the CAR and SAR models. *Journal of Statistical Planning and Inference* **121** 311–324.

WILBY, R. L., WIGLEY, T. M. L., CONWAY, D., JONES, P. D., HEWITSON, B. C., MAIN, J. and WILKS, D. S. (1998). Statistical downscaling of general circulation model output : A comparison of methods. *Water Resources Research* **34** 2995–3008.

J. HEWITT  
J. A. HOETING  
DEPARTMENT OF STATISTICS  
102 STATISTICS BUILDING  
COLORADO STATE UNIVERSITY  
FORT COLLINS, CO 80523-1877  
USA  
E-MAIL: [joshua.hewitt@colostate.edu](mailto:joshua.hewitt@colostate.edu)  
[jah@rams.colostate.edu](mailto:jah@rams.colostate.edu)

J. M. DONE  
E. TOWLER  
CAPACITY CENTER FOR CLIMATE AND WEATHER EXTREMES  
NATIONAL CENTER FOR ATMOSPHERIC RESEARCH (NCAR)  
P.O. BOX 3000  
BOULDER, CO 80307-3000  
USA  
E-MAIL: [done@ucar.edu](mailto:done@ucar.edu)  
[towler@ucar.edu](mailto:towler@ucar.edu)